Controlling the Relative Orientation of Reactants with Intermolecular Forces: Intermolecular State-Dependent Structure in Prereactive H_2−OH Complexes

David T. Anderson[†] and Marsha I. Lester*

Department of Chemistry, University of Pennsylvania, Philadelphia, Pennsylvania 19104-6323

Received: August 6, 2002; In Final Form: November 19, 2002

A theoretical study has been carried out to examine the orientation distribution functions of the OH and H_2 diatoms in various intermolecular states of the prereactive H_2−OH complex. Multidimensional quantum calculations have been conducted on a high-quality ab initio intermolecular potential energy surface to obtain the energies and body-fixed wave functions for the rovibrational states of H_2−OH. These calculations show that the H_2 and OH diatoms undergo nearly free internal rotation within the complex. However, the angular anisotropy of the intermolecular potential orients the OH and aligns the *ortho*-H_2 internal rotational motions within the complex. The relative orientation of the reactants is found to be well-defined and strongly intermolecular-state-dependent. Thus, by accessing different intermolecular states, the relative orientations of the reactants can be systematically manipulated. The degree of *body-fixed* orientation of OH in some bound states of H_2−OH, including the ground state of *ortho*-H_2−OH, approaches the highest degree of *space-fixed* orientation that has been achieved in hexapole orientation studies of OH. The experimental implications of the results are discussed.

I. Introduction

Electric field focusing has long been used to produce beams of oriented polar symmetric-top molecules.[1−4] Polar symmetric-top molecules can be manipulated using electric fields because they precess rather than tumble in certain rotational states, and as a result, they can maintain a constant projection of the molecular dipole moment on the electric field direction. The conventional approach is to use a hexapole electric field to select (focus) molecules in a single rotational state and then subsequently orient them in the laboratory frame with a modest homogeneous electric field. The orientation field serves only to define the space-fixed quantization axis for the state-selected molecular beam. In the orienting electric field, the symmetric-top molecules still exhibit precessional motion and retain most, if not all, of their zero-field quantum numbers. A great advantage of this venerable technique for producing oriented molecules is its state selectivity. If all of the molecules are in the same rotational state, they will respond similarly to the orienting field and thus produce a large net orientation of the molecules in the laboratory frame. In addition, by changing the focusing properties of the hexapole field, one can select rotational states with the highest degree of orientation (ones that strongly precess rather than tumble).

These types of hexapole orientation methods are applicable to the ground electronic state of OH X $^2\Pi$ because unquenched electronic angular momentum in the diatomic radical results in its rotational motion being similar to that of a polar symmetric top.[5−7] Interest in the stereodynamics of OH collisions, and radicals in general, has led to elegant studies of the inelastic scattering dynamics of oriented OH with H_2 and other collision partners.[7−10] These experiments have demonstrated that a high degree of OH orientation can be achieved in the laboratory frame using the hexapole method.[5−7] However, because the orientation of the collision partner and the impact parameter of the collision are still averaged quantities in these studies, it is desirable to develop new techniques that permit even greater control over the initial conditions of the collision.

This laboratory is exploring the possibility of orienting reactive collision partners by preparing them in specific rovibrational states of a weakly bound complex. For H_2−OH complexes, the production of such complexes is challenging because there is only a small barrier (2040 cm^{-1}) to the exothermic $H_2 + OH \rightarrow H_2O + H$ reaction.[11] Nevertheless, H_2−OH reactant complexes have been generated at sufficient number densities in a supersonic expansion to permit them to be characterized using rotationally resolved vibrational spectroscopy both in the OH overtone[12,13] and H_2 fundamental[14] regions. These spectra yield only limited information about the geometric structure of the complex, namely, the average separation between the centers of mass of the OH and H_2 partners and the projection of the total angular momentum (originating from unquenched angular momentum of the two diatoms) along the intermolecular axis.[12,13] The relative orientations of the H_2 and OH partners within the H_2−OH complex cannot be extracted from the spectroscopic data at the experimental resolution obtained (0.12 cm^{-1} in the near-infrared).

On the other hand, the relative orientations of the H_2 and OH partners within the H_2−OH complex can be predicted theoretically. Fortunately, H_2−OH has been the focus of first-principles quantum calculations that directly computed the H_2−OH infrared spectrum using a high-quality ab initio potential energy surface (PES).[15,16] There is close agreement between these theoretical results and experiment for the energies of the rovibrational lines in the infrared spectrum of H_2−OH.[12,13,17] This suggests that the calculated wave functions associated with the rovibrational states on this PES can be used to provide physical insight into the characteristics of the intermolecular

* Corresponding author: 215-573-2112 (fax), milester@sas.upenn.edu (e-mail).

[†] Present address: Department of Chemistry, University of Wyoming, Laramie, WY 82071-3838.

10.1021/jp021809w CCC: $25.00
Published on Web 03/21/2003

states of H_2-OH. Specifically, the relative orientations of the H_2 and OH partners in different intermolecular states of H_2-OH can be determined through an examination of the square modulus of the multidimensional wave function.

This paper shows that OH is strongly oriented in the body-fixed frame of the H_2-OH complex. In certain rovibrational states, the degree of OH orientation in the body-fixed frame of H_2-OH approaches the degree of space-fixed orientation that is achieved in hexapole studies of OH. In addition, the relative orientation of the H_2 and OH partners is well defined in *ortho*-H_2-OH (denoted hereafter as *o*-H_2-OH) and strongly intermolecular state dependent, even though both partners are undergoing nearly free internal rotation in the complex. These findings are consistent with the internal rotor dynamics of the related closed-shell species H_2-HF and H_2-HCl,[18−21] although the HX ($^1\Sigma$) molecule becomes oriented in these complexes by a different mechanism than the principal means identified for OH ($^2\Pi$). This difference will be discussed in detail (section IV.C), and stems from the pseudo-symmetric-top nature of the OH radical and its response to an electric field (first-order Stark effect).

The remainder of the paper is organized as follows. In section II, we describe the laboratory-fixed orientation of OH that is typically achieved in hexapole-state-selected experimental studies. In section III, we review the space-fixed bound-state calculations of H_2-OH,[15,16] which are then transformed into a body-fixed representation so that the relative angular orientations of H_2 and OH within the H_2-OH complex can be calculated. In section IV, we examine the calculated wave functions for different intermolecular bend states of *p*-H_2-OH and *o*-H_2-OH to obtain their "structures". We also examine the degree of orientation that can be achieved for selected quantum states to demonstrate that H_2-OH can be used to control the relative orientation of the reactants. Finally, in the last section, we formulate some conclusions based on this work.

II. Orientation of Hexapole-State-Selected Hydroxyl Radicals

This section overviews the degree of laboratory-fixed orientation that can be achieved for OH monomers in rotational states selected by an electrostatic hexapole. Specifically, we direct our attention to the shape of the OH rotational wave function in the orienting electric field that typically follows hexapole state selection. This background material serves to illustrate the degree of *space-fixed* orientation that can be achieved for OH radicals in such experiments and familiarize the reader with the form of the rotational wave functions for oriented OH radicals in their ground $^2\Pi$ electronic state. The same functional form will be used to quantify the degree of *body-fixed* orientation achieved in H_2-OH complexes in section IV.

In the absence of an electric field, the OH rotational wave functions are constructed from symmetric and antisymmetric combinations of symmetric-top wave functions

$$\Phi(j\omega m\epsilon) = \frac{1}{\sqrt{2}}(|j\omega m\rangle + \epsilon|j\ -\omega m\rangle) \qquad (1)$$

where $\epsilon = \pm 1$ is the space-fixed parity label ($\epsilon = +1$ for *e*-labeled states and -1 for *f*-labeled states).[22] For consistency with the discussion of the H_2-OH complex later, quantum numbers associated with the monomers are in lower case, and upper-case letters are reserved for quantum numbers associated with the complex. For simplicity, we label the OH quantum numbers using a pure Hund's case a notation, where j is the total angular momentum (including electronic and spin angular momentum) and ω and m are the molecule- and space-fixed projections of j, respectively. In a rotating OH diatom, the degeneracy of the *e* and *f* states is lifted, causing a small splitting between these states that is termed λ-doubling.

In a homogeneous electric field, however, parity is no longer well-defined, as the electric field mixes the two λ-doublet components of a given rotational level, yielding coupled wave functions

$$\Psi_1 = a\Phi(j\omega me) + b\Phi(j\omega mf)$$
$$\Psi_2 = -b\Phi(j\omega me) + a\Phi(j\omega mf) \qquad (2)$$

where the mixing coefficients (a, b) depend on the magnitude of the orienting electric field.[23] The Stark potential[24] created by the interaction of the dipole moment of OH (1.655 D)[25] with a typical laboratory orientation field (10 kV/cm) has a magnitude of $\sim$0.5 cm^{-1}. In the lower spin−orbit manifold the rotational energy spacing between the two lowest rotational levels ($j = {}^3/_2$ and $j = {}^5/_2$) is 88 cm^{-1}, whereas the λ-doublet energy spacing in the lowest ($j = {}^3/_2$) level is 3 orders of magnitude smaller at 0.055 cm^{-1}.[26] Thus, the Stark potential is not sufficient to induce substantial mixing of j levels, but it is adequate to mix the different parity components of the OH λ-doublet states and thereby orient OH. When the Stark shift of the states is much greater than the λ-doublet splitting, the coefficients in eq 2 reach their limiting values of $a = b = 1/\sqrt{2}$. In this "high-field" limit,[27] the OH rotational wave functions simplify to the corresponding symmetric-top wave functions[5]

$$|j\omega m\rangle = \left(\frac{2j+1}{4\pi}\right)^{1/2} D^{j*}_{m\omega}(\alpha,\beta) \qquad (3)$$

where α is the dihedral angle and β is the polar angle between the OH molecular axis ($\vec{z}$) and the space-fixed $\vec{Z}$ quantization axis (the $\vec{E}$ field direction). The analytical forms of the OH rotational wave functions are given by Wigner rotation matrices ($D^{j*}_{m\omega}$). Classically, the OH molecular axis precesses around the total angular momentum vector $\vec{j}$, which, in turn, precesses around the laboratory-frame quantization axis $\vec{Z}$. The highest degree of orientation of the OH radical is achieved in the high-field limit, and recent experimental studies of hexapole-state-selected OH radicals have essentially achieved this limit.[5−7]

The orientation distribution function for a given rotational state, denoted as $P_{j\omega m}(\beta)$, is defined as the probability that the OH molecular axis points at a certain polar angle β with respect to the laboratory-fixed electric field vector in the volume element $2\pi \sin\beta\ d\beta$. The orientation distribution function is evaluated from the square modulus of the wave function (eq 3) integrated over the dihedral angle (α). The classical recipe for calculating $P_{j\omega m}(\beta)$ has been given elsewhere,[28] and quantum calculations have also been published for various low-lying rotational states of OH.[5−7]

The degree of orientation that can be achieved for OH radicals in the $m = {}^3/_2$ and $m = {}^1/_2$ states of the lowest rotational level $|j\ \omega\ m\rangle = |{}^3/_2\ {}^3/_2\ m\rangle$ is illustrated in Figure 1. These probability distributions represent the high-field limit for a pure Hund's case a OH radical. The direction that the OH axis "points" depends on the relative sign of ω and m, and for simplicity, we consider only $|{}^3/_2\ \pm{}^3/_2\ \pm m\rangle$ states. In Figure 1, the orientation distribution function $P_{j\omega m}(\beta)$ is plotted in two equivalent ways: as a function of cos β from -1 to $+1$ (top panel) and as a polar plot as a function of β from 0° to 360° (bottom panel). Clearly, the $m = {}^3/_2$ and $m = {}^1/_2$ states have very different orientation

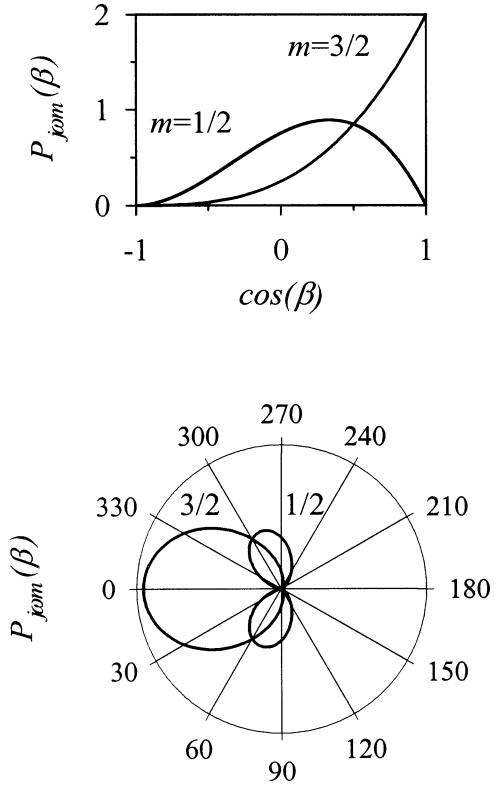

Figure 1. Calculated orientation distribution function $P_{j\omega m}(\beta)$ for OH in the state $|j\omega m\rangle = |^3/_2\ \pm^3/_2\ \pm m\rangle$. In these plots, β is the polar angle between the laboratory-fixed electric field vector and the OH bond axis. The top graph shows $P_{j\omega m}$ as a function of cos β, and the bottom graph displays $P_{j\omega m}$ in a polar plot. These distribution functions represent the high-field limit for hexapole orientation studies of OH.

distribution functions. $P_{j\omega m}(\beta)$ reaches a maximum at $\beta = 0°$ for the $m = {}^3/_2$ state, whereas the $m = {}^1/_2$ state has a node at this orientation. In addition, the $m = {}^3/_2$ distribution is more strongly peaked than the $m = {}^1/_2$ state, indicating a higher degree of orientation for the $m = {}^3/_2$ state. This is also consistent with a classical point of view, because j is more tightly constrained to precess around the electric field vector in the $m = {}^3/_2$ state.[22] Rotational states with $j = |\omega| = |m|$ achieve the highest degree of orientation because the OH rotational motion most closely resembles precession, as opposed to tumbling, in these states.

The average orientation of the OH radicals in the electric field can be readily evaluated in the high-field limit using[5,7]

$$\langle \cos\beta \rangle = \frac{m\omega}{j(j+1)} \tag{4}$$

The limiting values of $\langle\cos\beta\rangle$ for the $|j\ \omega\ m\rangle = |^3/_2\ \pm^3/_2\ \pm^3/_2\rangle$ and $|^3/_2\ \pm^3/_2\ \pm^1/_2\rangle$ states are 0.6 ($\beta = 53°$) and 0.2 ($\beta = 78°$), respectively. This high-field limit represents the highest degree of orientation of OH (without hybridization of the free-rotor levels, i.e., mixing of j) that can be achieved in a hexapole-state-selected orientation study. The fundamental limit to the degree of orientation originates in the quantum mechanical nature of the $|j\ \omega\ m\rangle = |^3/_2\ \pm^3/_2\ \pm^3/_2\rangle$ and $|^3/_2\ \pm^3/_2\ \pm^1/_2\rangle$ rotational states of OH (see Figure 1). In these states, j, ω, and m are good quantum numbers and only the e/f parity label of the λ-doublet components is lost.

III. Method

The procedure for calculating the body-fixed orientation of OH and H_2 in bound states of H_2-OH follows directly from that used in the last section for obtaining the space-fixed orientation of OH rotational states in an external electric field. The calculation begins with an evaluation of the energies and wave functions of the bound H_2-OH rovibrational states from quantum calculations on an accurate 4D intermolecular potential. For this, we use the ab initio potential[16] and computer code[15,16] developed by Clary, Werner, and co-workers. The resulting space-fixed wave functions are then transformed into the body-fixed frame and integrated numerically to obtain the orientation distribution functions for the OH and H_2 moieties in each rovibrational state of H_2-OH. In this section, we give the key equations that are used to compute the orientation distribution functions.

The potential energy function used in these calculations was developed by Miller and Clary on the basis of ab initio calculations by Kliesch and Werner.[16] These ab initio calculations consider only planar configurations of the H_2-OH complex. However, the fitted 4D intermolecular potential models out-of-plane configurations through an assumed functional form for the potential energy function that is based on electrostatics.[16] Another potential has been developed by Offer and van Hemert (OvH) that explicitly considers nonplanar configurations and fits their calculated ab initio points to a more flexible functional form.[29] It would be desirable to repeat the calculations reported here using the OvH potential to test the assumed functional form in out-of-plane configurations.

Using a variational approach, the rovibrational wave functions of H_2-OH are expanded in a product basis of angular (ang) and intermolecular stretch (str) basis functions

$$\Psi = \sum_{ij} c_{ij} \psi^i_{\text{ang}}\ \psi^j_{\text{str}} \tag{5}$$

The explicit form of the Hamiltonian and potential matrix in the space-fixed basis has been given previously.[15,16] All of the calculations presented here utilize an intermediate Hund's coupling case to accurately describe the contribution of the OH rotational wave functions, but we will neglect this added complexity in the equations that follow to be consistent with the previous section on the hexapole-state-selected orientation studies. The angular wave functions in eq 5 are expanded in a basis involving space-fixed diatom wave functions to give

$$\psi^{JMp}_{\text{ang}} = \sum_k c_k |j_{H_2} j_{OH} \omega_{OH} j_{12} L;\ JMp\rangle \tag{6}$$

with the H_2 and OH bond lengths fixed. Here, J refers to the total angular momentum (neglecting nuclear spin) of the complex with space-fixed projection M, L designates the end-over-end rotational angular momentum of the complex as a whole, and p indicates the total parity of the rovibrational wave function. The total angular momenta of the two diatoms, j_{H_2} and j_{OH}, are coupled tgether to form $j_{12} = j_{H_2} + j_{OH}$. In the H_2-OH bound-state calculations, spin−orbit coupling has been included in the description of the OH free-rotor states. Nevertheless, for simplicity, we label each state by ω_{OH}, which is rigorous only for Hund's case a coupling.

The space-fixed angular wave functions are defined as

$$|j_{H_2} j_{OH} \omega_{OH} j_{12} L;\ JMp\rangle = \sum_{m_{H_2} m_{OH} m_{12} m_L} \langle j_{H_2} m_{H_2}, j_{OH} m_{OH} | j_{12} m_{12}\rangle \langle j_{12} m_{12}, L m_L | JM\rangle \times |j_{H_2} m_{H_2}\rangle |j_{OH} \omega_{OH} m_{OH}\rangle |L m_L\rangle \tag{7}$$

where $\langle jm,\ ln|JM\rangle$ is a Clebsch−Gordan coefficient. Basis

functions that differ in J and p are decoupled. Thus, the eigenfunctions are calculated for a given value of J and p. The basis functions for the H_2 monomer $|j_{H_2}m_{H_2}\rangle$ and end-over-end rotation $|Lm_L\rangle$ of the H_2-OH complex are represented by spherical harmonics $Y_{lm}(\theta,\phi)$. The OH basis functions $|j_{OH}\omega_{OH}m_{OH}\rangle$ are represented by Wigner rotation matrices as defined in eq 3.

For calculations involving wave function properties instead of energies, smaller basis sets than are used in ref 16 can be employed. Here, the angular basis sets are constructed from space-fixed basis functions with maximum values of $j_{H_2} = 4$ for p-H_2, $j_{H_2} = 5$ for o-H_2, and $j_{OH} = {}^7/_2$ for OH. For both the p- and o-H_2-OH complexes, the stretching basis consists of 41 Gaussians equally spaced from 2 to 30 a_0. The product basis is then contracted to $n_{str} = 15$ and $n_{ang} = 35$ to give a product basis of 525 functions. The molecular parameters used in the calculations are taken from ref 16.

To visualize the wave functions, the space-fixed (SF) wave functions must be transformed into the body-fixed (BF) frame. The BF frame is defined with respect to the intermolecular axis $\vec{R}$, the vector connecting the center-of-mass of H_2 to the center-of-mass of OH. The unitary transformation between the space- and body-fixed basis sets is given by[15,16,30]

$$|j_{H_2}j_{OH}\omega_{OH}j_{12}L; JMp\rangle = \sum_{\bar{K}=1/2}\left(\frac{2[L]}{[J]}\right)^{1/2}\langle j_{12}\bar{K}, L0|J\bar{K}\rangle|j_{H_2}j_{OH}\omega_{OH}j_{12}K; JMp\rangle \quad (8)$$

where $\bar{K}$ is the magnitude of K, the projection of J on the body-fixed intermolecular axis $\vec{R}$, and $[J] = 2J + 1$. Note that K is often designated as P in treatments of open-shell complexes,[31] but for continuity with previous theoretical work on H_2-OH,[15,16] we will use K. The BF basis is defined in the standard way[15,16] as

$$|j_{H_2}j_{OH}\omega_{OH}j_{12}L; JMp\rangle = \sum_{k_{H_2},k_{OH}}\langle j_{H_2}k_{H_2}, j_{OH}k_{OH}|j_{12}K\rangle|j_{H_2}k_{H_2}\rangle|j_{OH}\omega_{OH}k_{OH}\rangle \quad (9)$$

where k_{H2} and k_{OH} are the projections of j_{H_2} and j_{OH}, respectively, onto the intermolecular axis and $k_{H_2} + k_{OH} = K$. The coefficients (bf_k) of the body-fixed angular wave functions $|j_{H_2}k_{H_2}\rangle|j_{OH}\omega_{OH}m_{OH}\rangle$ are thus the product of the space-fixed coefficients c_k (see eq 6) and the appropriate Clebsch−Gordan coefficients summed over the total space-fixed basis set. In the BF basis, the wave function is written in terms of the vectors $\vec{r}_{H_2} \equiv (\theta_{H_2}, \phi_{H_2})$ and $\vec{r}_{OH} \equiv (\theta_{OH}, \phi_{OH})$ that describe the orientation of the two diatoms with respect to the intermolecular axis $\vec{R}$. The angle θ is the polar angle, and ϕ is the dihedral angle, with ($\theta_{H_2} = 0°$, $\theta_{OH} = 0°$) defined as the linear HH−HO configuration and ($\phi_{H_2} = 0°$, $\phi_{OH} = 0°$) indicative of a planar structure.

To examine the body-fixed orientation of the OH diatom within the complex, the H_2-OH rovibrational wave function is integrated numerically (Gauss−Legendre and Gauss−Hermite quadrature) over the intermolecular stretch coordinate and three of the four angular coordinates

$$P(\theta_{OH}) = \int\Psi^*_{str}\Psi_{str}\,dR\int\int\int\Psi^*_{ang}\Psi_{ang}\sin\theta_{H_2}\,d\theta_{H_2}\,d\phi_{H_2}\,d\phi_{OH} \quad (10)$$

This integration gives the orientation distribution function $P(\theta_{OH})$. The integration over θ_{H_2} can be replaced by an integration over θ_{OH} to obtain the corresponding orientation distribution function for the H_2 diatom within the complex, $P(\theta_{H_2})$. The quantity $P(\theta)$ represents the probability of finding the OH (or H_2) bond axis at a polar angle θ with respect to the intermolecular axis $\vec{R}$ in the solid angle $2\pi\sin\theta\,d\theta$. As an internal check, the transformed angular eigenfunctions were found to be orthonormal, verifying that the SF → BF transformation and the analytical forms of the basis functions were properly implemented in the computer code.

As a final note, we mention that the effects of unresolved hyperfine structure due to nuclear spin in the molecules are not included in the present analysis. Zare and co-workers have treated the dynamics of nuclear-spin-coupling effects on diatomic molecules aligned via polarized laser excitation.[32] These studies show that precession of the nuclear spin leads to a decrease of the initial molecular alignment, particularly for low-j states where the magnitude of the nuclear spin is significant in comparison. For example, such nuclear hyperfine depolarization effects overwhelm the laboratory-frame alignment dynamics for HF molecules prepared in low-j states.[32] However, in this case, where the nuclear spin coupling is weak, the intermolecular potential should be sufficient to decouple the nuclear spin angular momenta.[6] Thus, although the nuclear hyperfine couplings were neglected in the present study, we expect that the orientation distribution functions calculated in this work would be qualitatively preserved even if nuclear hyperfine couplings were included.

IV. Results

Nuclear motions of the H_2 and OH moieties in H_2-OH sample two different potential energy surfaces because of the electronic degeneracy of the OH X $^2\Pi$ partner. The two potentials are degenerate for linear geometries of the H_2-OH complex, but for nonlinear geometries, the degeneracy is lifted, resulting in two adiabatic electronic potentials. For planar configurations of the complex, these surfaces are denoted as $V_{A'}$ and $V_{A''}$ depending on whether the half-filled pπ orbital of OH lies in or out of the H_2-OH plane, respectively. For studies involving couplings between monomer wave functions, such as inelastic scattering or bound-state calculations, it has been shown to be more convenient to work with diabatic potentials defined as the *average* $V_{AVG} = {}^1/_2(V_{A'} + V_{A''})$ and *difference* $V_{DIF} = {}^1/_2(V_{A''} - V_{A'})$ potentials.

The average intermolecular potential is characterized by a relatively high degree of angular anisotropy, and it is this potential anisotropy that serves to orient the rotating diatoms in the body-fixed frame of the complex. The global minimum (-188 cm^{-1}) on V_{AVG} is located at a T-shaped geometry where the H atom of OH points toward the H_2 diatom ($\theta_{H_2} = 90°$, $\theta_{OH} = 0°$) with a center-of-mass separation of 3.22 Å.[16] At this global minimum, the barriers to internal rotation of the H_2 or OH monomers are 470 and 210 cm^{-1}, respectively. Because the lowest rotational-level spacings of the H_2 and OH monomers are quite large, 360 and 88 cm^{-1}, one anticipates only weak mixing between *different* j levels and, consequently, nearly free-rotor behavior for the H_2 and OH diatoms in the complex. However, the angular anisotropy in V_{AVG} is sufficient to lift the $2j + 1$ orientational degeneracy of a given j level, generating $2j + 1$ distinct body-fixed k states. Each k state corresponds to a different projection of the diatom angular momentum j onto the intermolecular axis. It is this angular anisotropy that leads to orientation of the OH radical and alignment of the H_2 partner, specifically for o-H_2, in the BF frame of the H_2-OH complex.

A. *para*-H_2-OH. We anticipate that the p-H_2 molecule will retain its $j_{H_2} = 0$ quantum number in the p-H_2-OH complex making it effectively spherical. As a result, the intermolecular

TABLE 1: Leading Coefficients (bf_k) of the Body-Fixed Angular Wave Functions in the Expansion $|j_{H_2}\ k_{H_2}\rangle|j_{OH}\ \omega_{OH}\ k_{OH}\rangle$ for the Dominant ψ_{ang} of p-H_2−OH[a]

j_{H_2}	k_{H_2}	j_{OH}	k_{OH}	$v_b = 0$	$v_b = 1$	$v_b = 2$	$v_b = 3$
0	0	$^3/_2$	$+^3/_2$	0.8985		0.1518	
0	0	$^3/_2$	$+^1/_2$	0.2545	0.7655	0.3883	0.6176
0	0	$^3/_2$	$-^1/_2$	−0.0726	0.6210	−0.5969	−0.7662
0	0	$^3/_2$	$-^3/_2$	0.2953		−0.6680	
			$\Sigma(bf)^2$ [b]	0.9645	0.9716	0.9763	0.9685
			energy[c]	−26.3	−21.0	−15.3	−14.5
			$\langle\cos\theta_{OH}\rangle$[d]	+0.479	+0.115	−0.330	−0.103
			K[e]	$+^3/_2$	$+^1/_2$	$-^3/_2$	$-^1/_2$

[a] Reported values are for the lowest possible J level and $p = +$ for each intermolecular bend v_b state. [b] Sum of the squares of the four indicated body-fixed coefficients. [c] Intermolecular energy (cm^{-1}) with respect to dissociation. [d] Average body-fixed orientation of OH. The limiting values of $\langle\cos\theta_{OH}\rangle$ for pure OH rotor states are +0.6 for $|j_{OH}\ \omega_{OH}\ k_{OH}\rangle = |^3/_2\ \pm^3/_2\ \pm^3/_2\rangle$ and +0.2 for $|j_{OH}\ \omega_{OH}\ k_{OH}\rangle = |^3/_2\ \pm^3/_2\ \pm^1/_2\rangle$. [e] Approximate K quantum label for each intermolecular bend state.

bend states of p-H_2−OH should resemble those of rare gas−OH complexes, such as Ar−OH.[31,33,34] In this case, there will be four bound intermolecular bend states that correspond to the four $(2j_{OH} + 1)$ possible body-fixed projections of the $j_{OH} = {}^3/_2$ free rotor ($k_{OH} = +^3/_2, +^1/_2, -^1/_2, -^3/_2$). The sign of k_{OH}, which refers to its sign relative to ω_{OH} (assumed to be positive), indicates whether the H end (positive k_{OH}) or the O end (negative k_{OH}) of OH points toward H_2.

Analysis of the total wave function for p-H_2−OH reveals that only one product function contributes significantly (i.e., $c_{00} \approx 1$ and $\Psi = \psi_{ang}\psi_{str}$). Furthermore, only a few of the BF angular basis functions contribute to ψ_{ang}. The leading coefficients bf_k of the body-fixed angular wave functions for the four intermolecular bend states of p-H_2−OH are presented in Table 1. The quantum number $v_b = 0-3$ is used to designate the energetic ordering of these states. Each state is also labeled by the approximate quantum number K that denotes the projection of J on the intermolecular axis. Examination of Table 1 reveals that the angular wave functions for these four bend states are constructed (>95%) from linear combinations of the four body-fixed basis functions with $j_{H_2} = 0$ and $j_{OH} = {}^3/_2$, $\omega_{OH} = {}^3/_2$. Contributions from higher j_{H_2} or j_{OH} free-rotor states (or from the upper OH spin−orbit state $\omega_{OH} = {}^1/_2$) to the angular wave functions of the weakly bound complex are minimal. Note that because relatively small variational basis set expansions were used in this study, the intermolecular energies presented in Table 1 are only approximate as energies converge more slowly than wave function properties. Furthermore, a detailed comparison with the published results of Clary and co-workers[16] is difficult because these researchers reported energies for $J = {}^3/_2$ and $p = +$ only, whereas we present the energy of the lowest possible J state for each intermolecular state (e.g., $J_{min} = {}^1/_2$ for $K = {}^1/_2$ states). However, calculations carried out in this laboratory with large basis sets are in quantitative agreement with the earlier published results of Clary and co-workers.[16]

The angular wave function for the ground intermolecular state ($v_b = 0$) of p-H_2−OH is primarily composed [to greater than 80% $(0.8985)^2$] of a single body-fixed term with $j_{H_2} = 0$, $k_{H_2} = 0$ and $j_{OH} = {}^3/_2$, $\omega_{OH} = {}^3/_2$, $k_{OH} = +^3/_2$ (see Table 1). The H_2 and OH orientation distribution functions for this state are shown in Figure 2. The plot of $P(\theta_{H_2})$ vs $\cos(\theta_{H_2})$ is constant, as expected for an essentially pure $j_{H_2} = 0$ state, illustrating that the H_2 is isotropically distributed over all possible angular orientations. The plot of $P(\theta_{OH})$ vs $\cos(\theta_{OH})$ shows that OH is preferentially oriented with its H end pointed toward H_2 ($\cos\theta_{OH} \approx +1$), as expected for a $k_{OH} = +^3/_2$ state. The most favorable orientation for OH is analogous to that at the global minimum on V_{AVG}. For comparison, $P(\theta_{OH})$ for a pure $|j_{OH}\ \omega_{OH}\ k_{OH}\rangle = |^3/_2\ \pm^3/_2\ \pm^3/_2\rangle$ state is also plotted (dotted line) in Figure 2. The good agreement between the two distribution functions demonstrates that the OH moiety in the ground intermolecular state of p-H_2−OH is well described by a single body-fixed wave function.

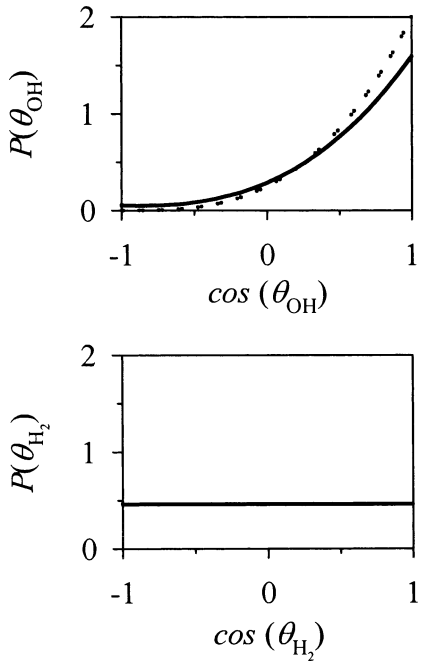

Figure 2. Body-fixed orientation distribution functions $P(\theta)$ for OH and H_2 in the ground intermolecular state of p-H_2−OH. In these plots, θ is the polar angle between the body-fixed intermolecular axis and the diatom bond axis. Whereas H_2 is isotropically distributed, OH is preferentially oriented with the H end pointing toward the H_2. The degree of orientation of OH approaches the pure $k_{OH} = {}^3/_2$ state limit (dotted line), which is included for comparison.

The agreement between the two $P(\theta_{OH})$ distributions shown in Figure 2 is not perfect, however, because the OH moiety is not in a pure $k_{OH} = {}^3/_2$ state in the ground intermolecular bend state of p-H_2−OH. Different k_{OH} (or equivalently K) states are mixed into the angular wave function by off-diagonal ($\Delta k_{OH} = \pm 1$) Coriolis couplings, which are induced by end-over-end rotation of the complex. These couplings make k_{OH} only an approximate quantum number, although Figure 2 shows that the body-fixed k_{OH} quantum number still provides a physically meaningful quantum label for the ground intermolecular state of p-H_2−OH. The comparison can be made more quantitative by calculating the average orientation cosine of the OH moiety. In the ground intermolecular state of p-H_2−OH, the average orientation of OH is $\langle\cos\theta_{OH}\rangle = +0.479$ as compared to $\langle\cos\theta_{OH}\rangle = +0.6$ for a pure $|j_{OH}\ \omega_{OH}\ k_{OH}\rangle = |^3/_2\ \pm^3/_2\ \pm^3/_2\rangle$ quantum state. These differences stem from k_{OH} state mixing and not from the rigorous treatment of spin−orbit interactions in OH. The contribution from the upper $^2\Pi_{1/2}$ spin−orbit state is only ~0.03%.

The orientation distribution functions for the four bound intermolecular bend states of p-H_2−OH are shown as polar plots in Figure 3. Note that the $P(\theta)$ functions shown in Figure 2 for the ground intermolecular state of p-H_2−OH are replotted in Figure 3 as polar plots. The $P(\theta_{H_2})$ functions do not change with intermolecular state because the H_2 diatom is in nearly a pure $j_{H_2} = 0$ free-rotor state in each case. On the other hand, $P(\theta_{OH})$ changes for each intermolecular bend state because these

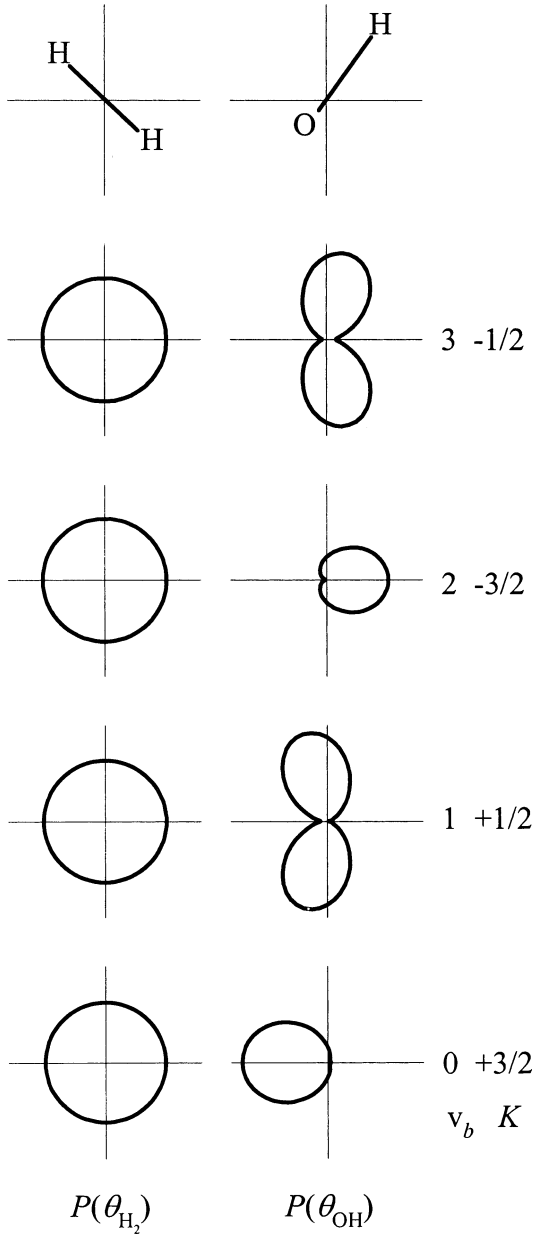

Figure 3. Polar plots of orientation distribution functions $P(\theta_{H_2})$ and $P(\theta_{OH})$ for the four intermolecular bend states of p-H_2−OH. The approximate quantum numbers v_b and K are used to label each state. The H_2 molecule is spherical as expected for $j_{H_2} = 0$, whereas the OH diatom displays four different body-fixed orientations.

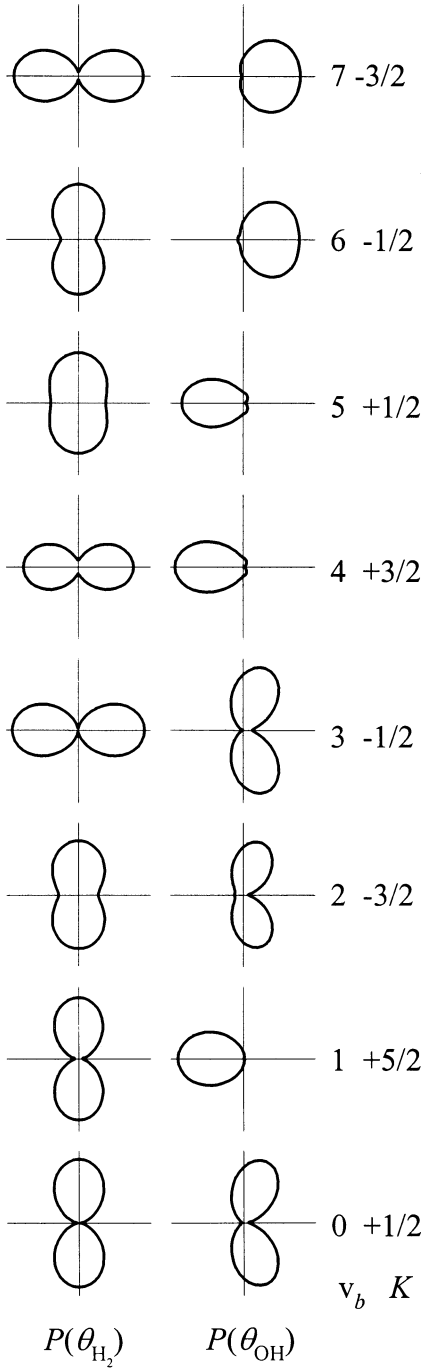

Figure 4. Polar plots of orientation distribution functions $P(\theta_{H_2})$ and $P(\theta_{OH})$ for the eight lowest-energy intermolecular bend states of o-H_2−OH. The approximate quantum numbers v_b and K are used to label each state. The H_2 can be aligned either parallel or perpendicular to the intermolecular axis. The OH diatom displays roughly three types of orientation: with the H end pointed toward H_2, with the O end toward H_2, and with the OH radical aligned perpendicular to the intermolecular axis.

four states correspond to the $(2j_{OH}+1) = 4$ different body-fixed projections of a $j_{OH} = {}^3/_2$, $\omega_{OH} = {}^3/_2$ free rotor. To a large degree, the energy spread and energetic ordering of these four bend states is a measure of the OH angular anisotropy in V_{AVG}. The different body-fixed orientations of OH preferentially sample different regions of the intermolecular potential and accordingly have different intermolecular energies.

The $P(\theta_{OH})$ functions shown in Figure 3 for the excited bend states ($v_b = 1-3$) of p-H_2−OH appear to derived from distinct k_{OH} terms, yet inspection of Table 1 shows that several k_{OH} body-fixed basis functions contribute to each excited bend state. As discussed earlier, Coriolis couplings cause the mixing of k_{OH} basis functions. These couplings do not completely "wash-out" the body-fixed orientation of OH in the complex, but they do diminish the distinctions between different intermolecular bend states. For example, the mean OH orientation cosine $\langle \cos \theta_{OH} \rangle$ in the ground intermolecular state is close to the limiting value, but the values for the excited bend states are substantially less than the values for a pure $|j_{OH}\ \omega_{OH}\ k_{OH}\rangle$ body-fixed state (Table 1). Nevertheless, the intermolecular potential does cause a substantial degree of body-fixed orientation for OH within the p-H_2−OH complex that differs for the various bend states. The degree of OH orientation in p-H_2−OH is similar to that achieved in Ar−OH.[33,34] On the other hand, the p-H_2 ($j_{H_2} = 0$) partner remains essentially spherical in p-H_2−OH and is neither oriented nor aligned by the intermolecular potential.

TABLE 2: Leading Coefficients (bf_k) of the Body-Fixed Angular Wave Functions for the Dominant ψ_{ang} of *o*-H_2−OH[a]

j_{OH}	k_{OH}	j_{H_2}	k_{H_2}	$v_b = 0$	$v_b = 1$	$v_b = 2$	$v_b = 3$	$v_b = 4$	$v_b = 5$	$v_b = 6$	$v_b = 7$
$^3/_2$	$+^3/_2$	1	+1		−0.9532						
$^3/_2$	$+^3/_2$	1	0		−0.1524	−0.2129		−0.8666			−0.0545
$^3/_2$	$+^1/_2$	1	+1		−0.0027	0.0242		0.2132			0.1192
$^3/_2$	$+^3/_2$	1	−1	−0.1242	−0.0270	0.0133	−0.0296	−0.1472	−0.8380	−0.2017	0.0219
$^3/_2$	$+^1/_2$	1	0	0.0166	−0.0025	0.0052	−0.0729	0.0214	0.3512	0.1678	−0.0254
$^3/_2$	$-^1/_2$	1	+1	0.9681	0.0659	−0.2793	0.1106	−0.0928	0.1226	0.0353	−0.464
$^3/_2$	$+^1/_2$	1	−1	−0.0709	0.0113	0.0400	−0.0754	−0.0306	−0.0303	0.0833	0.0528
$^3/_2$	$-^1/_2$	1	0	0.1224	0.0045	0.2749	−0.9612	0.0883	0.0223	−0.1733	0.0380
$^3/_2$	$-^3/_2$	1	+1	−0.0288	−0.0029	−0.0044	−0.1744	0.0209	−0.2454	0.8911	0.2393
$^3/_2$	$-^1/_2$	1	−1		−0.0396	0.8807		−0.2882			0.0288
$^3/_2$	$-^3/_2$	1	0		−0.0081	0.0637		0.0865			−0.8981
$^3/_2$	$-^3/_2$	1	−1		0.0765						
			$\Sigma(bf_k)^2$[b]	0.9738	0.9402	0.9810	0.9784	0.9269	0.9023	0.9011	0.8887
			energy[c]	73.2	77.5	81.9	83.2	88.8	93.1	100.4	110.0
			$\langle\cos\theta_{OH}\rangle$[d]	−0.173	+0.550	−0.136	−0.196	+0.444	+0.382	−0.400	−0.416
			K[e]	$+^1/_2$	$+^5/_2$	$-^3/_2$	$-^1/_2$	$+^3/_2$	$+^1/_2$	$-^1/_2$	$-^3/_2$

[a] Reported values are for the lowest possible J level and $p = +$ for each intermolecular bend v_b state. [b] Sum of the squares of the 12 indicated body-fixed coefficients. [c] Intermolecular energy (cm^{-1}) with respect to the $j_{H_2} = 0$, $j_{OH} = ^3/_2$ dissociation limit. [d] Average body-fixed orientation of OH. The limiting values of $\langle\cos\theta_{OH}\rangle$ for pure OH rotor states are +0.6 for $|j_{OH}\ \omega_{OH}\ k_{OH}\rangle = |^3/_2\ \pm^3/_2\ \pm^3/_2\rangle$ and +0.2 for $|j_{OH}\ \omega_{OH}\ k_{OH}\rangle = |^3/_2\ \pm^3/_2\ \pm^1/_2\rangle$. [e] Approximate K quantum label for each intermolecular bend state.

B. *ortho*-H_2−OH. The intermolecular bend states of *o*-H_2−OH are remarkably different from those of *p*-H_2−OH. The $j_{H_2} = 1$ rotor of *o*-H_2 can be aligned with respect to the body-fixed intermolecular axis in *o*-H_2−OH, whereas the $j_{H_2} = 0$ rotor in *p*-H_2−OH is spherically distributed. This alignment of *o*-H_2 also leads to a higher degree of orientation for the OH partner in the *o*-H_2−OH complex. In general, *o*-H_2 complexes have a greater number of bound intermolecular bend states that are spread over a larger energy range than the analogous *p*-H_2 complexes.[20] This is due to the greater orientational degeneracy of the $j_{H_2} = 1$ free-rotor state as well as the increased anisotropy arising from two bend (both OH and H_2) coordinates.

The orientation distribution functions for the lowest eight bound intermolecular states of *o*-H_2−OH are plotted in Figure 4. The leading body-fixed coefficients bf_k for these intermolecular states are also given in Table 2. These intermolecular bend states correspond to different body-fixed orientations of the $j_{H_2} = 1$ and $j_{OH} = ^3/_2$, $\omega_{OH} = ^3/_2$ rotors. The ground intermolecular state of *o*-H_2−OH is primarily composed of one body-fixed combination (∼94%), namely, $k_{H_2} = +1$ and $k_{OH} = -^1/_2$, indicating that both the H_2 and OH diatoms lie perpendicular to the intermolecular axis. Note that the OH orientation cosine has a value $\langle\cos\theta_{OH}\rangle = -0.173$, which is very close to the limiting value of $\langle\cos\theta_{OH}\rangle = -0.2$ for a pure $|j_{OH}\ \omega_{OH}\ k_{OH}\rangle = |^3/_2\ \pm^3/_2\ \mp\ ^1/_2\rangle$ state.

The excited bend states shown in Figure 4 can also be reasonably well described (∼70−92%) by a single body-fixed term (see Table 2). For example, the wave function for the first excited bend state ($v_b = 1$) of *o*-H_2−OH can be constructed (∼91%) from a single body-fixed combination with $k_{OH} = +^3/_2$ and $k_{H_2} = +1$. In the $v_b = 1$ state, the OH orientation cosine is $\langle\cos\theta_{OH}\rangle = 0.550$, which is very close to the limiting value of 0.600 for a pure $|j_{OH}\ \omega_{OH}\ k_{OH}\rangle = |^3/_2\ \pm^3/_2\ \pm^1/_2\rangle$ state. Intermolecular bend states with predominantly $k_{OH} = \pm^3/_2$ character result in head or tail orientation of OH with respect to the BF axis, such as $v_b = 1$ and $v_b = 4-7$. A sideways orientation of OH in the BF frame is obtained in intermolecular bend states with primarily $k_{OH} = \pm^1/_2$ character, such as $v_b = 0$ and $v_b = 2-3$. Even for a pure $|j_{OH}\ \omega_{OH}\ k_{OH}\rangle$ state, however, the degree of OH orientation in *o*-H_2−OH depends principally on the intrinsic nature of the $k_{OH} = \pm^3/_2$ or $k_{OH} = \pm^1/_2$ rotational state. States with $k_{OH} = \pm^3/_2$ have more strongly peaked orientation distribution functions than states with $k_{OH} = \pm^1/_2$ (see section II). As a result, the highest degree of OH body-fixed orientation is achieved in *o*-H_2−OH bound states with OH in a nearly pure $k_{OH} = \pm^3/_2$ states, e.g., $v_b = 1$.

The orientation or alignment of both partners can be specified in *o*-H_2−OH, as compared to only the OH partner in *p*-H_2−OH. For many of the bound states of *o*-H_2−OH, the degree of alignment of *o*-H_2 approaches the pure $j_{H_2} = 1$ state limit, with $k_{H_2} = 0$ or $k_{H_2} = \pm 1$ indicating whether *o*-H_2 is aligned along or perpendicular to the BF axis, respectively. This can be seen in Figure 4, where the $P(\theta_{H_2})$ distribution functions closely resemble the well-known p-orbital shape of a pure $j_{H_2} = 1$ free rotor.

The relative orientation of the two partners in *o*-H_2−OH is strongly dependent on the intermolecular bend state, as illustrated in Figure 4. The $j_{OH} = ^3/_2$ and $j_{H_2} = 1$ internal rotors have distinctly different projections on the body-fixed intermolecular axis, k_{OH} and k_{H_2}, in the various intermolecular states (Table 2). This gives rise to enormously different relative orientations of the partners or structures for the various intermolecular bend states of *o*-H_2−OH. Furthermore, because most of the *o*-H_2−OH states are well described by a single body-fixed term, this represents the highest degree of reagent orientation that can be achieved without hybridization (mixing j) of the rotational states of the individual partners.

We note that the structure of the ground intermolecular bend state of *o*-H_2−OH, with both *o*-H_2 and OH positioned perpendicular to the intermolecular axis, is significantly different from the T-shaped H_2−OH geometry at the global minimum on V_{AVG}. This is a surprising result because the lowest-energy intermolecular state would be expected to sample the global potential minimum preferentially. This suggests that the unquenched angular momentum in the *o*-H_2−OH system, originating from both *o*-H_2 and OH moieties, influences the structure of these weakly bound complexes. In previous work,[12,13] we had assumed a T-shaped ground-state structure for *o*-H_2−OH rather than the nearly parallel configuration of the OH and H_2 diatoms shown in Figure 4. Although good agreement was found between the infrared transition frequencies of *o*-H_2−OH observed experimentally and those calculated by Clary and co-workers,[16] the preferred structure of the ground intermolecular state accessed in these studies only became apparent after careful examination of the body-fixed wave functions.

The infrared spectrum of the *o*-H_2−OH complex in the OH overtone region has previously been reported[13] and is reproduced here in Figure 5 for a discussion of the relative orientation of

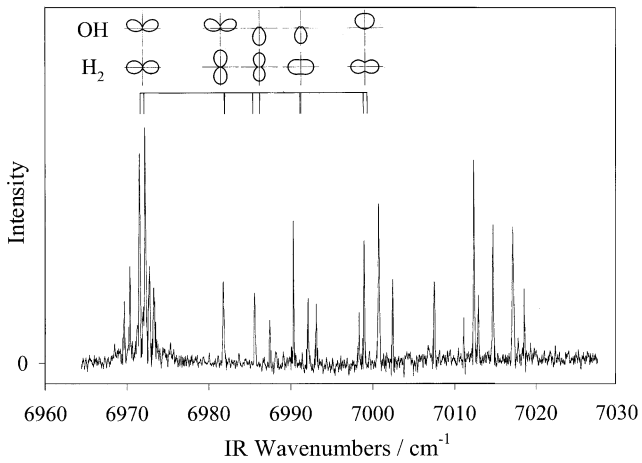

Figure 5. Infrared spectrum of the *o*-H_2−OH complex in the OH overtone region reproduced from ref 13. The lowest-energy feature at 6971.9 cm^{-1} has been assigned as the pure overtone band, and higher-energy transitions are combination bands involving the simultaneous excitation of the OH overtone and intermolecular bending vibrations. The ticks show the calculated line positions for the lowest allowed Q-branch transitions. The computed orientational distribution functions for the bending states access by infrared excitation of *o*-H_2−OH are displayed above the ticks (also see Figure 4).

the reactants in the intermolecular states that are accessed experimentally. The most intense feature in the infrared spectrum is the pure OH overtone stretch at 6971.9 cm^{-1} (band origin), which is shifted by 0.6 cm^{-1} to higher energy from that of uncomplexed OH. The rotational structure of the pure overtone stretch is dominated by a strong central Q-branch with a large parity splitting. This band has been assigned as a $K = {}^1/_2 \leftarrow {}^1/_2$ band of *o*-H_2−OH according to a detailed comparison with ab initio theory.[13,16] The structure the ground intermolecular state of the *o*-H_2−OH complex ($v_b = 0$) with both *o*-H_2 and OH positioned perpendicular to the intermolecular axis is shown above the pure overtone stretch in Figure 5.

As discussed in ref 13, approximately 20 additional rovibrational transitions have been observed up to 60 cm^{-1} higher in energy than the pure overtone origin. These rovibrational transitions arise from combination bands involving the simultaneous excitation of two quanta of OH stretch and intermolecular bend (v_b) vibrations. On the basis of comparison with ab initio calculations (with calculated line positions for the lowest allowed Q-branch transitions shown as ticks), the first combination band at 6981.8 cm^{-1} has been assigned to overlapping parity components of the $Q({}^1/_2)$ transitions that terminated on an excited $K = -{}^1/_2$ bending level ($v_b = 3$). The computed structure for this excited bending state shows that *o*-H_2 is preferentially aligned along the intermolecular axis. The next higher energy combination band has been assigned to a $K = {}^3/_2 \leftarrow {}^1/_2$ band with the transitions at 6985.6 and 6987.4 cm^{-1} assigned to the parity split $Q({}^3/_2)^-$ and $Q({}^3/_2)^+$ lines. Theory predicts an excited intermolecular bending state ($v_b = 4$) with $K = {}^3/_2$ at approximately this energy with OH pointing toward *o*-H_2 and both partners oriented along the intermolecular axis. Yet higher combination bands have been assigned as transitions to the $v_b = 5$ and 6 intermolecular bending states. The computed orientational distribution functions for these bending states are also displayed in Figure 5. We did not attempt to assign or compute structures for the remaining transitions to higher energy as these are most likely due to intermolecular bending (and possibly stretching) states near the dissociation limit. Thus, the calculations indicate that infrared excitation of the *o*-H_2−OH complex can be used to access intermolecular bend states (in combination with OH overtone stretch) with enormously different relative orientation of the partners. The ramification of these different orientations has been observed in the vibrational predissociation dynamics of D_2−OH, where the OH fragments exhibit a striking λ-doublet preference, revealing alignment of the unpaired pπ orbital with respect to the OH rotation plane, which changes with the intermolecular state selected.[35]

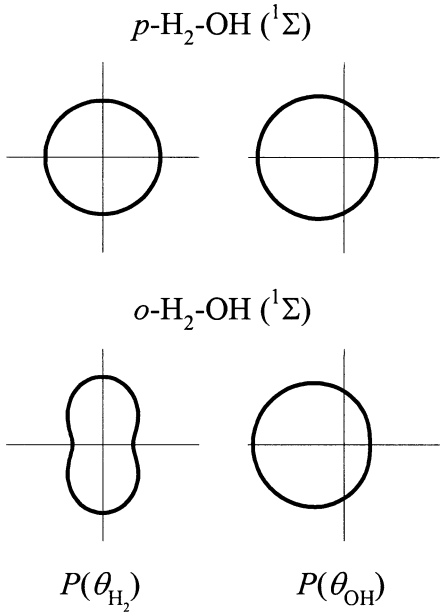

Figure 6. Polar plots of orientation distribution functions $P(\theta_{H_2})$ and $P(\theta_{OH})$ for the ground intermolecular bend state of the hypothetical closed-shell *p*-H_2−OH (top) and *o*-H_2−OH (bottom) complexes. The degree of OH orientation is significantly reduced compared to the open-shell calculations presented in earlier figures. See text for details.

C. $^2\Pi$ Nature of OH. The $^2\Pi$ nature of the OH radical has a profound influence on the degree of body-fixed orientation that can be achieved in H_2−OH complexes. The unquenched electronic and spin angular momenta cause the rotational motion of OH to be more akin to that of a symmetric top than to that of a closed-shell diatomic rotor. As a result, the OH radical's rotational motion is more easily perturbed by the approach of the H_2 diatom than it would be if it were a closed-shell diatom. Stated another way, the precessional motion of a symmetric top is more easily oriented by angular anisotropy in V_{AVG} than the tumbling motion of a closed-shell diatom.

To demonstrate how differently a hypothetical OH ($^1\Sigma$) closed-shell diatom would respond to the intermolecular forces of H_2−OH, the bound-state calculations were repeated on the same potential energy surface (V_{AVG}) using a closed-shell Hamiltonian[20] with OH ($^1\Sigma$) free-rotor states ($B_{OH} = 18.5$ cm^{-1}) represented by spherical harmonics. Because the lowest rotational state of this hypothetical OH ($^1\Sigma$) is $j_{OH} = 0$, the OH diatom remains essentially spherical in H_2−OH complexes. The closed-shell version of the OH moiety can become oriented in the BF frame of the complex only if the anisotropy of the intermolecular potential is sufficient to induce j_{OH} state mixing. The orientation distribution functions computed for the ground intermolecular states ($v_b = 0$) of *p*- and *o*-H_2−OH (closed-shell OH) are plotted in Figure 6. The degree of OH orientation in both cases is substantially reduced compared to the distributions displayed earlier (Figures 3 and 4). The OH diatom is more strongly oriented when it is explicitly treated as an open-shell $^2\Pi$ molecule than as a closed-shell $^1\Sigma$ diatom, even though the calculations were performed on identical potential energy surfaces. In addition, the closed-shell calculations predict a T-shaped ground-state structure for *o*-H_2−OH with the H-atom

of OH pointing toward H_2 (Figure 6). By contrast, the proper treatment of OH as $^2\Pi$ in the open-shell calculations reveals that both H_2 and OH lie perpendicular to the intermolecular axis in the ground state of *o*-H_2−OH (Figure 4).

The mechanism by which the OH diatom becomes oriented in the H_2−OH complex is very different depending on whether OH is taken to be in a $^2\Pi$ or $^1\Sigma$ electronic state. For a closed-shell OH ($^1\Sigma$) diatom, the degree of OH orientation depends on j_{OH} state mixing, which is related to the ratio of the OH monomer rotational spacing and the effective barrier to rotation in the complex. Because the j_{OH} spacing is large, a significant amount of angular anisotropy in V_{AVG} would be needed to orient an OH ($^1\Sigma$) diatom. In contrast, OH ($^2\Pi$) becomes oriented in H_2−OH by an electrostatic-induced mixing of the parity components of the OH λ-doublet states. Because the λ-doublet splitting is much smaller than the rotational energy spacing, a smaller degree of angular anisotropy is required to orient the OH ($^2\Pi$) internal precessional motion. Thus, open-shell OH ($^2\Pi$) can be more easily oriented in the H_2−OH complex than if it were a closed-shell diatom ($^1\Sigma$). The different sensitivities with which the two types of rotational motions (precession vs tumbling) respond to electrostatic perturbations has long been recognized in the context of the response of polar molecules to a uniform electric field.[36] In a perturbation approach, polar symmetric-top molecules have a first-order Stark effect, whereas polar diatomic molecules interact with the field only in second order.[36]

The different mechanisms by which $^2\Pi$ and $^1\Sigma$ diatoms become oriented in weakly bound complexes underscores an important distinction between H_2−OH and H_2−HX (X = F, Cl) complexes. The closed-shell H_2−HX systems have also been the focus of high-level PES calculations and bound-state calculations.[20,21,37] In the closed-shell species, the HX diatom becomes oriented by j_{HX} state mixing induced by the intermolecular potential. The degree of orientation in the *o*-H_2−HX ground intermolecular state can be relatively high; for example, it is calculated[21] to be $\langle \cos \theta_{HX} \rangle = 0.684$ in *o*-H_2−HCl and experimentally measured to be $\langle \cos \theta_{HX} \rangle = 0.743$ in *o*-H_2−HF.[38] In the ground state of H_2−HF or H_2−HCl, the j_{HX} state mixing is sufficient to consider the HX internal angular motion as large-amplitude librational motion. The j_{HX} state mixing mechanism also implies that the excited intermolecular bend states of H_2−HX will not display the same amount of variability in structure as seen in Figure 4 for *o*-H_2−OH.

D. Effect of Overall Rotation on Orientation. The highest degree of orientation is achieved for the lowest possible rotor level J of each H_2−OH intermolecular bend state. There are two main reasons for this. First, an increase in end-over-end rotation of the complex will increase off-diagonal Coriolis interactions that tend to mix different body-fixed orientations. Second, as the end-over-end rotational of the complex increases, the effective anisotropy of the intermolecular potential will not be adequate to keep the OH and H_2 internal rotational motions oriented and aligned, respectively, in the body-fixed frame. As an example, consider the impact of increasing the end-over-end rotation on the ground-state properties of *o*-H_2−OH. The H_2 and OH orientation distribution functions are plotted for this $K = +1/2$ state as a function of J ($J \geq 1/2$) in Figure 7. As J increases, the peaks and nodes in the H_2 and OH distribution functions become less well defined. In this specific case, the increased rotation has a greater effect on the H_2 alignment than on the OH orientation. Thus, for stereodynamic studies where the highest degree of orientation of the constituents is desirable, the lowest J level should be selected.

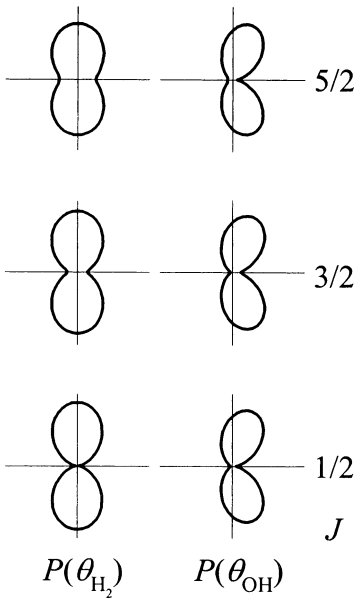

Figure 7. Polar plots of orientation distribution functions $P(\theta_{H_2})$ and $P(\theta_{OH})$ for the ground intermolecular bend state of *o*-H_2−OH as a function of the total angular momentum of the complex, J. As J increases, the degree of body-fixed orientation of both H_2 and OH is diminished. In general, the highest degree of orientation for a given intermolecular state is attained in the lowest possible J state.

E. Effect of V_{DIF}. The calculations presented thus far have included the effects of the difference potential, because both V_{AVG} and V_{DIF} were used in the bound-state calculations. The calculations were repeated with V_{AVG} only to ascertain the impact of V_{DIF} on the orientation distribution functions for H_2 and OH. The primary effect of V_{DIF} is to cause small energy splittings between rovibrational states with the same total angular momentum J but different total parity. The orientation distribution functions are thus only marginally changed for different parity states with the same J, even when the parity splitting is large ($\sim$1 cm^{-1}). (The distributions plotted in the figures are for total $p = +$ states.) Thus, V_{DIF} is found to have very little effect on the absolute energies or structures of the bound states of H_2−OH.

V. Discussion

This paper demonstrates that intermolecular forces can be used to orient the OH radical in weakly bound complexes such as H_2−OH and contrasts the degree of orientation achieved with that obtained using conventional hexapole-based techniques. Hexapole state selection uses a hexapole field to select OH radicals in a particular m level and subsequently orients these molecules in the space-fixed laboratory frame using an electric field. A large net orientation of a sample of OH molecules results from state selection and the propensity of certain OH rotor states to be strongly oriented by an electric field. The highest degree of OH orientation is achieved in the high-field limit for the $|j_{OH}\ \omega_{OH}\ k_{OH}\rangle = |^3/_2\ \pm^3/_2\ \pm^3/_2\rangle$ rotational state. The quantum calculations presented here show that OH can be oriented to a similar degree with respect to the *body-fixed frame* in *o*-H_2−OH. In *o*-H_2−OH, the OH molecule is in a nearly pure rotational state that maintains a constant projection of j_{OH} on the intermolecular axis. Accordingly, the form or shape of the OH internal rotor wave function in H_2−OH is very similar to that of OH in an external electric field. The OH radical maintains a constant body-fixed projection (k_{OH}) in H_2−OH, whereas in the hexapole studies, it maintains a constant space-fixed projection (m_{OH}). The major difference between the two approaches is that

the orientation is specified with respect to two different axis systems.

The intermolecular bound states of H_2-OH offer many scenarios for controlling the relative orientation of OH and H_2. In p-H_2-OH, the H_2 molecule is isotropically distributed over all possible angular geometries and therefore appears spherical to OH. The OH radical, on the other hand, is oriented in the body-fixed frame of the complex. This allows for studies of the interaction of an oriented OH molecule (either head-on or sideways) with p-H_2 ($j_{H_2} = 0$) by accessing different intermolecular bend states. In o-H_2-OH, by contrast, there is a high degree of OH orientation and H_2 alignment. The BF orientation and alignment are a direct consequence of the unquenched angular momentum in both partners, whose free-rotor internal motions create anisotropic spatial distributions of the partners that sample different regions of the intermolecular PES. As shown in this work, the intermolecular bend states are well described in terms of different body-fixed projections of the $j_{H_2} = 1$ and $j_{OH} = {}^3/_2$ internal rotors. Although the OH and o-H_2 monomers are undergoing nearly free internal rotation, the rotational motions of both partners are quantized with respect to the intermolecular axis of the complex, and thus the relative orientation of the reagents is well-defined.

The body-fixed alignment of o-H_2 and orientation of OH in o-H_2-OH also indicate that the relative spatial orientation of the reagents can be changed dramatically with intermolecular bend excitation. By accessing the different bend states, the o-H_2 alignment and OH orientation can be changed in discrete steps of k_{H_2} and k_{OH}. The different relative orientations of the H_2 and OH partners in the various intermolecular bend states sample different regions of the PES and accordingly have intermolecular energies that differ by tens of wavenumbers. The relative orientation of the H_2 and OH partners can therefore be systematically manipulated by exciting different intermolecular states.

Our interest is to use the bound states of H_2-OH as the initial states in vibrationally mediated half-collision studies of H_2-OH. The ground-state H_2-OH complexes are formed in a supersonic expansion and then vibrationally excited using high-power, narrow-line-width laser sources. This combination allows for precise species selection because binary complexes of p-H_2-OH or o-H_2-OH can be preferentially excited (they absorb at slightly different frequencies). Second, we have shown that H_2-OH complexes can be prepared state-selectively with two quanta of OH stretch[12,13] or one quantum of H_2 stretch.[14] Third, this excitation is stereospecific because the initial relative orientation of the partners is restricted by the bound-state wave function. Finally, excitation of single rovibrational states allows the total angular momentum of the system to be specified. Experimental studies have demonstrated that the ground intermolecular state be prepared via pure OH overtone excitation and, in addition, excited intermolecular bend states can be accessed via combination (intramolecular + intermolecular) band excitation.[13] The quantum calculations presented here are used to predict the structure of H_2-OH in the states prepared in these experiments, and this information can be used to interpret state-to-state dynamical studies. There is experimental evidence that the OH products from vibrational predissociation of D_2-OH retain some memory of their initial state in the complex, as demonstrated by the dissimilar OH fine-structure distributions resulting from different intermolecular states.[35] By preparing intermolecular bend states in which the relative orientation of the H_2 and OH partners resembles the bent transition state structure for the OH + H_2 hydrogen abstraction reaction,[11] the probability of reactive decay is likely to be enhanced, but the extent of such enhancement is still unknown.

Acknowledgment. We thank David C. Clary (University College, London) for supplying us with the intermolecular potential and bound-state computer programs used in this work. This research was principally supported by the Chemistry Division of the National Science Foundation. Acknowledgment is also made to the donors of the Petroleum Research Foundation, administered by the ACS, for partial support of this research.

References and Notes

(1) Bulthius, J.; van Leuken, J. J.; Stolte, S. *J. Chem. Soc., Faraday Trans.* **1995**, *91*, 205−214.
(2) Brooks, P. R. *J. Phys. Chem.* **1993**, *97*, 2153−2157.
(3) Friedrich, B.; Pullman, D. P.; Herschbach, D. R. *J. Phys. Chem.* **1991**, *95*, 8118−8129.
(4) Parker, D. H.; Berstein, R. B. *Annu. Rev. Phys. Chem.* **1989**, *40*, 561−595.
(5) Hain, T. D.; Curtiss, T. J. *J. Phys. Chem. A* **1998**, *102*, 9696−9701.
(6) Hain, T. D.; Weibel, M. A.; Backstrand, K. M.; Curtiss, T. J. *J. Phys. Chem. A* **1997**, *101*, 7674−7683.
(7) Schreel, K.; ter Meulen, J. J. *J. Phys. Chem. A* **1997**, *101*, 7639−7647.
(8) van Beek, M. C.; ter Meulen, J. J.; Alexander, M. H. *J. Chem. Phys.* **2000**, *113*, 637−646.
(9) van Beek, M. C.; Berden, G.; Bethlem, H. L.; ter Meulen, J. J. *Phys. Rev. Lett.* **2001**, *86*, 4001−4004.
(10) van Beek, M. C.; ter Meulen, J. J. *J. Chem. Phys.* **2001**, *115*, 1843−1852.
(11) Alagia, M.; Balucani, N.; Casavecchia, P.; Stranges, D.; Volpi, G. G.; Clary, D. C.; Kliesch, A.; Werner, H.-J. *Chem. Phys.* **1996**, *207*, 389−409.
(12) Schwartz, R. L.; Anderson, D. T.; Todd, M. W.; Lester, M. I. *Chem. Phys. Lett.* **1997**, *273*, 18−24.
(13) Anderson, D. T.; Schwartz, R. L.; Todd, M. W.; Lester, M. I. *J. Chem. Phys.* **1998**, *109*, 3461−3473.
(14) Wheeler, M. D.; Todd, M. W.; Anderson, D. T.; Lester, M. I. *J. Chem. Phys.* **1999**, *110*, 6732−6742.
(15) Miller, S. M.; Clary, D. C. *J. Chem. Phys.* **1993**, *98*, 1843−1855.
(16) Miller, S. M.; Clary, D. C.; Kliesch, A.; Werner, H.-J. *Mol. Phys.* **1994**, *83*, 405−428.
(17) Wheeler, M. D.; Anderson, D. T.; Lester, M. I. *Int. Rev. Phys. Chem.* **2000**, *19*, 501−529.
(18) Lovejoy, C. M.; Nelson, D. D., Jr.; Nesbitt, D. J. *J. Chem. Phys.* **1987**, *87*, 5621−5628.
(19) Lovejoy, C. M.; Nelson, D. D., Jr.; Nesbitt, D. J. *J. Chem. Phys.* **1988**, *89*, 7180−7188.
(20) Clary, D. C.; Knowles, P. J. *J. Chem. Phys.* **1990**, *93*, 6334−6349.
(21) Anderson, D. T.; Schuder, M.; Nesbitt, D. J. *Chem. Phys.* **1998**, *239*, 253−269.
(22) Zare, R. N. *Angular Momentum: Understanding Spatial Aspects in Chemistry and Physics*; Wiley: New York, 1988.
(23) Townes, C. H.; Schawlow, A. L. *Microwave Spectroscopy*; Dover: New York, 1975.
(24) Moore, D. T.; Oudejans, L.; Miller, R. E. *J. Chem. Phys.* **1999**, *110*, 197−208.
(25) Nelson, D. D., Jr.; Schiffman, A.; Nesbitt, D. J. *J. Chem. Phys.* **1989**, *90*, 5455−5465.
(26) Coxon, J. A. *Can. J. Phys.* **1980**, *58*, 933−949.
(27) The high-field limit of hexapole-state-selection experiments is to be distinguished from the yet higher fields that are used in brute-force methods to mix j levels and create pendular states.
(28) Choi, S. E.; Bernstein, R. B. *J. Chem. Phys.* **1986**, *85*, 150−160.
(29) Offer, A. R.; van Hemert, M. C. *J. Chem. Phys.* **1993**, *99*, 3836−3846.
(30) Launay, J. M. *J. Phys. B* **1977**, *10*, 3665−3672.
(31) Dubernet, M.-L.; Flower, D.; Hutson, J. M. *J. Chem. Phys.* **1991**, *94*, 7602−7618.
(32) Altkorn, R.; Zare, R. N.; Greene, C. H. *Mol. Phys.* **1985**, *55*, 1−9.
(33) Bonn, R. T.; Wheeler, M. D.; Lester, M. I. *J. Chem. Phys.* **2000**, *112*, 4942−4951.
(34) Chakravarty, C.; Clary, D. C. *J. Chem. Phys.* **1991**, *94*, 4149−4160.
(35) Todd, M. W.; Anderson, D. T.; Lester, M. I. *J. Phys. Chem. A* **2000**, *104*, 6532−6544.
(36) Rost, J. M.; Griffin, J. C.; Friedrich, B.; Herschbach, D. R. *Phys. Rev. Lett.* **1992**, *68*, 1299−1302.
(37) Krause, P. J.; Clary, D. C. *Mol. Phys.* **1998**, *93*, 619−625.
(38) Jucks, K. W.; Miller, R. E. *J. Chem. Phys.* **1987**, *87*, 5629−5633.